RSC Advances

PAPER

View Article Online
View Journal | View Issue

Cite this: *RSC Adv.*, 2022, **12**, 6641

Preparation of mussel-inspired silver/polydopamine antibacterial biofilms on Ti–6Al–4V for dental applications

Hongmei Zhao,[ab] Na Bai,[ab] Qian Zhang,[ab] Ying Wang,[ab] Wenjing Jiang[ab] and Jianjun Yang *[ab]

Received 3rd September 2021
Accepted 22nd February 2022

DOI: 10.1039/d1ra06634j

rsc.li/rsc-advances

The properties of osseointegration and antibacterial ability is vital import for dental materials. Herein, we designed the multilayer TC4–Ag–polydopamine coatings, to provide TC4 with slow-release antibacterial properties whilst maintaining cytocompatibility. In brief, thickness of Ag inner layer can be easily controlled by magnetron sputtering technology. The resulting top polydopamine layer protected the Ag well from corrosion and gave a sustained release of Ag^+ up to one month. In addition, the prepared TC4–Ag–polydopamine samples with Ag thickness of 20 and 30 nm, showed high hydrophilic performance with the contact-angle less than 20°, low cytotoxicity and good cytocompatibility. Expectedly, it could become a prospective candidate for future slow-release antibacterial dental materials.

Introduction

Titanium is the most preferred material for artificial joints, bone trauma products and dental implants because of its good biocompatibility and corrosion resistance properties.[1–4] However, after implantation the surface does not have antibacterial ability and is prone to bacterial adhesion and biofilm formation, which can lead to infection or peri-implantitis and even treatment failure.[5–8] Peri-implantitis is one of the main complications of implant restoration failure, which is characterized by the formation and deepening of periodontal pockets, progressive resorption of bone tissue, and even loosening and loss of the implant. Studies have shown that peri-implantitis pathogenic bacteria originate from the oral environment.[9] Therefore, it is important to enhance the osseointegration ability of the material surface and give the surface antibacterial ability for implant application.

Various surface modification methods have been proposed to grant excellent antimicrobial activity to the implants to improve their success rate.[10–12] Inorganic antimicrobial agents such as silver, copper and zinc have good antimicrobial activity.[13] They are widely incorporated into the implant surface to obtain the desired antimicrobial properties without the risk of bacterial resistance. Silver is widely used in the medical and health field because of its good bactericidal and anti-inflammatory properties, non-resistant and non-cytotoxic at appropriate doses.[14–16] Among the broad-spectrum antimicrobial agents, silver has the advantages of high antimicrobial capacity, high stability, and does not trigger bacterial resistance.[17,18] However, silver is also toxic to mammalian cells when the concentration is too high[19] including the fibroblasts involved in wound healing where the toxic concentration of Ag^+ is 50 mg L^{-1}.[20] Therefore, silver-loaded, slow-release antimicrobial implant coatings have become a highly visible topic due to their continuous release of silver ions or atoms for antimicrobial and antibacterial purposes, thus avoiding infections.

The mussel-like adhesive dopamine molecule has catechol and amino groups, which can polymerize themselves to form polydopamine with more reactive groups.[21,22] It firmly adheres to numerous material surfaces to improve biocompatibility and enables bridging of other biomolecules on the material surface; it can also chelate and even reduce metal ions.[23–25] These properties make it an important choice for surface modification of implants. In recent years, researchers have used the excellent properties of dopamine, combined with antibacterial agent, to prepare a variety of antimicrobial coatings.[26–28] Liao[29] first deposited polydopamine on polyimide (PI) films, and then deposited silver nanoparticles (AgNPs) onto the PI films through the reducing ability of polydopamine to form highly antimicrobial PI films. Vincent[30] dipped polystyrene modified with polydopamine into silver nitrate solution to obtain silver nanoparticles by the same principle and confirmed its excellent antibacterial ability. Fu[31] developed an antimicrobial Ti coating that has great potential as a dental implant material. In the experiment, the Ti substrate was pre-modified with a dopamine coating, and then metronidazole was immobilized on the surface of the dopamine-modified Ti substrate. Jia[32] developed a trap-killing system in their research, the Ti slow-release antimicrobial coatings were prepared by firmly immobilizing AgNPs on the dopamine surface through tight physicochemical

[a]*The Affiliated Hospital of Qingdao University, Qingdao 266003, China. E-mail: yjjqd@126.com*
[b]*School of Stomatology of Qingdao University, Qingdao 266003, China*

interactions. However, to date studies about the polydopamine Ti slow-release antimicrobial coatings are mainly focused on TiO_2–polydopamine–AgNPs structure. But in the TiO_2–polydopamine–AgNPs film, AgNPs is still on the surface of the film, it would have more opportunity to be released. Therefore, in this study we designed a new structure of TiO_2–AgNPs–polydopamine to produce a antibacterial coatings with longer antimicrobial release time.

Magnetron sputtering is an effective technology to produce stable quality thin films at a high deposition rate.[33] In order to obtain good quality of antimicrobial coatings, the nano silver film was deposited on titanium discs by direct magnetron sputtering. After that, polydopamine coating developed *in situ* onto Ag film *via* covalent cohesion. In this way, a rigid Ti(TiO_2)–Ag–polydopamine coating can be easily built on Ti.

Materials and methods

Preparation and characterization of Ti–Ag–polydopamine coatings

Commercially available TC4 (Ti–6Al–4V) discs with a size of diameter = 15 mm, thickness = 1 mm was mechanically sprayed by 50 μm Al_2O_3 at a rate of 3 kg m^{-2} for 1 minute, and then following by acid etching (37% HCl : 98% H_2SO_4 : H_2O = 1 : 1 : 2) in 60 °C for 10 min. Sequentially the treated Ti discs were rinsed by ultrasonication in deionized water, acetone, ethanol, and DI.

After that Ag thin films were deposited onto TC4 discs by using a DC magnetron sputtering system (JCP-350, TECHNOL), the schematic diagram is shown in Fig. 1(b). Deposition parameters are shown in Fig. 1(a). In this study all the samples were deposited with Ag film at three different thickness of 10, 20 and 30 nm. Film thickness was controlled by an online measurement system calibrated by post-deposition measurements with the Alpha-Step 500 (Tencor) surface profiling system and by scanning electron microscopy (JSM-7800F, JEOL) for film cross-section observation. After Ag deposition, the Ti–Ag treated samples were subjected to 2 mg mL^{-1} dopamine hydrochloride (Alfa Aesar) in Tris–HCl buffer (10 mM, pH = 8.5; Sigma) for 24 h under constant vibration at 37 °C, with the Ag-coated side facing up. Then thoroughly ultra-sonicated to detach excess monomer and particles. The TC4 samples after the Ag magnetron sputtering process and polydopamine coating treatment are developed into slow-release antimicrobial samples. The TC4–Ag samples with different Ag layers are designated as Ti–Ag10, Ti–Ag20 and Ti–Ag30; correspondingly the TC4–Ag–polydopamine samples with different Ag layers are designated as PDA10, PDA20 and PDA30 in the subsequent discussion.

The PDA coated systems as TC4–Ag–polydopamine samples will be identified from this point forwards as PDA samples. The morphology and microstructure of Ti, Ti–Ag and PDA samples were investigated by using a Phenom Pro scanning electron microscope (Phenom Pro SEM, Germany). The crystal structure of the coatings was characterized by X-ray diffractometer (Rigaku SmartLab) using Cu Kα radiation ($\lambda = 0.154$ nm) (45 kV at 200 mA) at X'celerator normal mode between 2θ of 20° and 80°. For compositional analysis, energy-dispersive X-ray spectrometry (EDS), and ATR-FTIR spectroscopy (Nicolet iS5, Thermo Scientific) were employed.

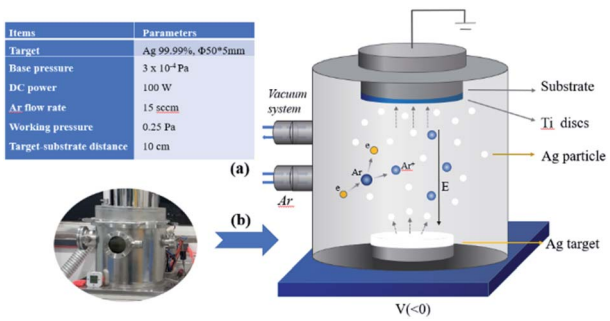

Fig. 1 The deposition parameters (a) and schematic diagram (b).

Contact angle (CA) measurements

Static contact angle was measured on a contact angle goniometer (JY-PHb). A drop of distilled water of 5 μL volume was placed on the sample, and the contact angle was measured by holding the water drop on the treated sample surface for 60 seconds. All the CA values were tested and reported as the mean of five measurements. In the CA measurements, before testing the prepared samples would be separated into two groups. One will be put in stand atmosphere situation and another group would be immersed in DI water, both groups would be tested after 24 hour and 1 week.

Ag^+ release into phosphate buffer solution (PBS)

To investigate the release behavior of Ag^+ ions from Ti–Ag and PDA coatings, specimens ($n = 3$) were immersed in 6 mL of PBS for one month at 37 °C,[32] and the entire volume of solution was collected at predetermined time points and refilled with fresh PBS accordingly. After that the collected buffer solution would be analyzed using inductively coupled plasma-atomic emission spectrometry (ICP-OES, PerkinElmer Avio200, USA), the release profiles and rates of Ag^+ were determined. In addition, the total Ag content was calculated by dissolving the coating in 4% dilute nitric acid.

Antibacterial test

The antibacterial activity of the Ti–Ag and PDA samples ($n = 3$) was determined by zone of inhibition (ZOI) experiments utilizing Gram-positive bacteria *Staphylococcus aureus* (*S. aureus*) and Gram-negative bacteria *Escherichia coli* (*E. coli*). Samples were placed face down on solid agar medium evenly coated with bacteria (20 μL, 10^6 CFU mL^{-1}). After incubation at 37 °C for 24 hours, the areas of microbial growth inhibition (clear areas around the samples) were photographed to indicate the antimicrobial capacity of the various sample surfaces.

Cell assessment

Cell culture. A murine calvaria osteoblastic precursor cell line (MC3T3-E1) was obtained from the Cell Culture Center of

Shanghai Institutes for Biological Science Chinese Academy of Sciences (Shanghai, China). MC3T3-E1 cells (passage 6–8) were cultured and expanded in basal medium containing DMEM (Biological Industries, Israel) supplemented with 10% FBS (Biological Industries, Israel) and 1% penicillin/streptomycin (Biological Industries, Israel) at 37 °C with 5% CO_2 in the air.

Cytotoxicity assessment. Cells were co-cultured with TC4, PDA10, PDA20 and PDA30 samples to determine their effects on cell adhesion. All the samples were placed in a 12-well plate and the MC3T3-E1 cells were seeded on the samples with the density of 4×10^4 cells per well and cultured for 24 h. Subsequently, discard the cell culture medium and rinse the sample three times with PBS solution to remove loosely adherent cells. Afterward, the cells on the samples were fixed with 4% para-formaldehyde solution at RT for 20 min. The cell membranes were then treated with 0.5% Triton X-100 (Sigma-Aldrich) solution for 3 min. The cells were subsequently stained with DAPI and TRITC-phalloidin (Solarbio, China) for the nucleus and cytoskeleton, respectively. Images were taken by inverted fluorescence microscopy (Nikon A1 MP, Japan). ImageJ software was used to quantify the cell spreading area and elongation.

Cellular viability was measured using a CCK-8 (Med Chem Express, Shanghai). Briefly, MC3T3-E1 cells were seeded onto TC4, PDA10 PDA20 and PDA30 samples in a 12-well plate at a density of 4×10^4 cells per well. Afterward, 10 μL of CCK-8 reagent solution with 200 μL of new medium was added to each well of the plate using a repeating pipette at 1, 3, 5, and 7 days, respectively. After incubation for another 2 h, OD_{450} was measured using a microplate reader. The TC4 is used for the control sample in the cellular viability test. The experiment was performed in triplicate and repeated three times independently.

Results and discussion

Surface morphology analysis

The SEM images of Ti–Ag and PDA samples with different Ag thickness are shown in Fig. 2. As shown in the figure, all the samples retained the rough surface after sandblasting and acid etching due to the thin silver nanofilms plated, providing a basis for later clinical applications. In Fig. 2(a–c), visible particles were observed from the SEM images, and the particle size and shape of the particles varied with the thickness of the inner deposited Ag layer. This proves the preliminary success of the dopamine polymerization grafting experiment, and the specific composition of the particles will be further analyzed and proven in the following sections. Researchers report that the evolution of the Ag films is consistent with the Volmer–Weber model, in which the growth of nuclei leads to the formation of islands, which then coalesce into a continuous film. The critical thickness for Ag atoms to form a continuous dense film is around 10 nm. Since the surface of the Ti sheet is not as flat as glass in this experiment, the deposited Ag film might be as an uneven silver net at 10 nm in this study. The shape of the underlying deposited Ag film, as presented in SEM pictures, influenced the dopamine particles' shape. When inner deposited Ag layer was 10 nm, the produced dopamine particles were small; while the other two groups of samples produced large dopamine particles, which is estimated to further affect the performance of the slow-release antimicrobial coatings.

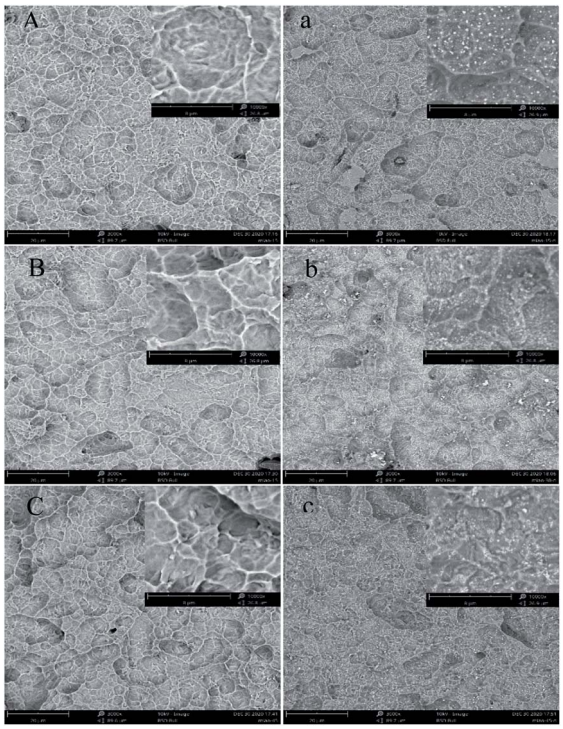

Fig. 2 SEM images of Ti–Ag ((A) 10, (B) 20, (C) 30) and PDA ((a) 10, (b) 20, (c) 30) samples.

XRD analysis

XRD spectra of the TC4, Ti–Ag and PDA samples with different Ag inner layer thickness are shown in Fig. 3. Ag was analysed according to JCPDS card no. 04-0783, TC4 is an alloy there is no standard card for it, it was analysed according to different Ti.[34] According to the XRD results, none of Ag peaks had been found when the Ag layer was 10 nm in both Ti–Ag and PDA samples.

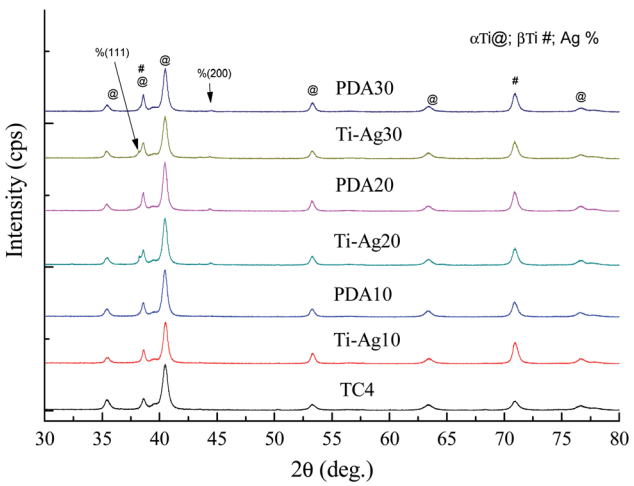

Fig. 3 XRD spectra of the TC4, Ti–Ag and PDA samples.

This is probably due to the fact that the Ag layer has not yet formed a continuous film at the thickness of 10 nm. The Ag (111) and (200) peaks can be detected in Ti–Ag samples when the Ag layer thickness was 20 nm and 30 nm, which means the Ag layer has formed a continuous film at that thickness. However, the Ag XRD information was becoming a little weak after the coating of polydopamine on the surface, especially the Ag (111). Which maybe caused by the interfering of polydopamine, but the Ag (200) peak still proved the exiting of Ag film. In a word, the deposition of Ag inner layer and polymerization of dopamine top layer on TC4 did not alter the XRD patterns largely.

EDS analysis

EDS spectra of the Ti–Ag30 and PDA samples with different Ag inner layer thickness are shown in Fig. 4. The doped elements such as Al, V and Fe, *etc.* have not been tested in the EDS testing. For the convenience of calculation, the elements doped in TC4 in EDS experiment are not counted. For example, the peak of aluminium element, which was obvious near 1.48 keV, was not calculated in the results. After calculated in this way, it was found that Ag and Ti were the major elements of the Ti–Ag30 sample. After polymerization of dopamine, obvious C, N and O elements can be detected in PDA samples, which had not been found in Ti–Ag sample. This was indirect evidence that dopamine had been deposited onto the surface of the Ag layer. The EDS spectrum also revealed that the percentage of Ag in the overall elements content of the PDA samples increased as the thickness of the Ag layer increasing. Although EDS can only be used for qualitative or semi-quantitative analysis, the silver content data would provide some foundation for the later antibacterial testing.

FTIR analysis

The FTIR spectra of the prepared Ti–Ag and PDA samples are shown in Fig. 5. As we can see in Fig. 5(A), at approximately 3726 cm^{-1} the stretching vibrations of –OH was detected, which may be caused by the absorbed of water in the air by the Ti–Ag thin films. In Fig. 5(B), the absorption around 3622 cm^{-1} was assigned to phenolic hydroxyl stretching vibrations of catechol groups, whereas the peaks around 1616 and 2101 cm^{-1} corresponded to the stretch vibrations of aromatic rings and C=C groups. The peaks of 1701 and 2101 cm^{-1} were the stretch vibrations of C=O. The N–H shearing vibration of the amide group was evident at 1560 cm^{-1}. These results might prove the expected polydopamine was deposited. According to other researchers,[35,36] polydopamine and silver film are associated *via* forces of metal coordination, electron and electrostatic interactions. Correlating these with the SEM, XRD and FTIR results, one can conclude that a TC4–Ag–polydopamine composite

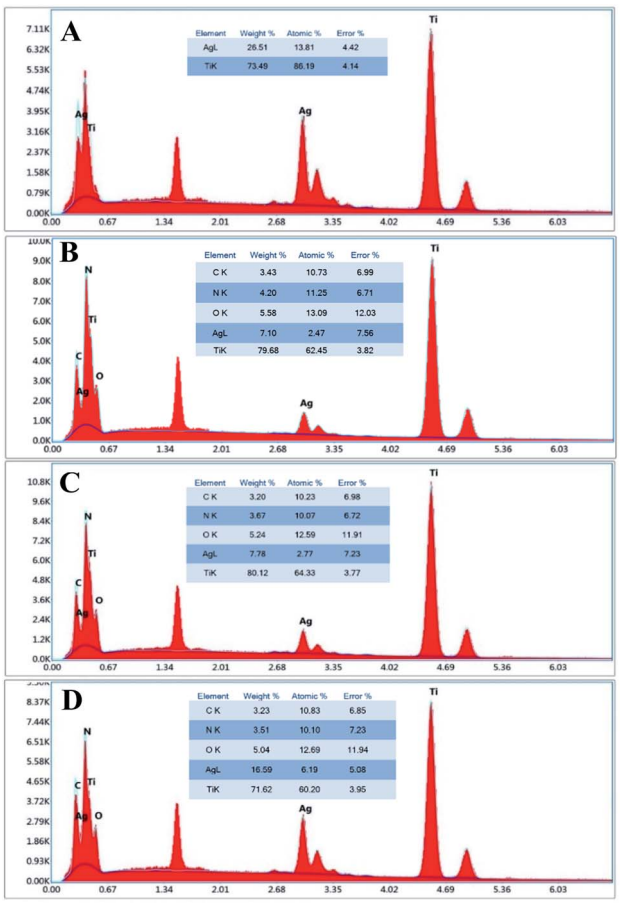

Fig. 4 EDS spectra of the Ti–Ag and PDA samples: (A) Ti–Ag30, (B) PDA10, (C) PDA20, (D) PDA30.

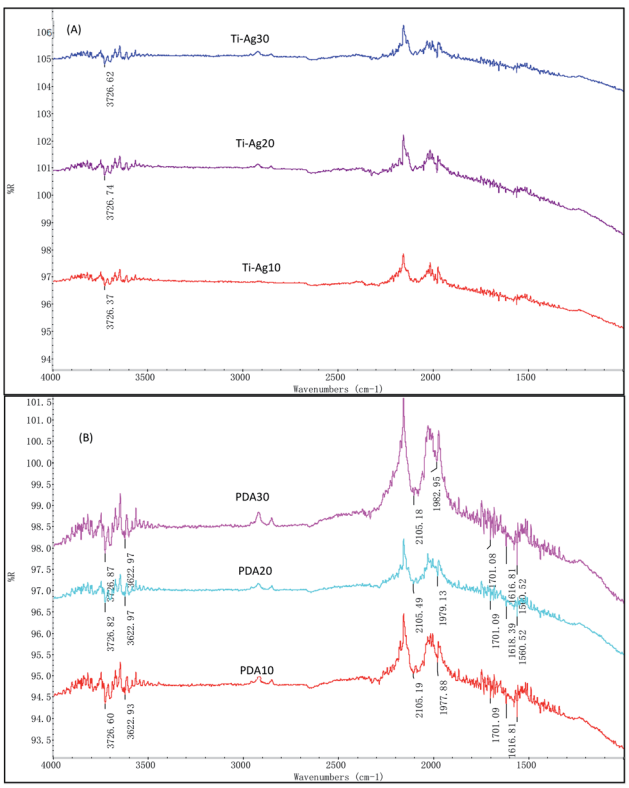

Fig. 5 FTIR spectra of the prepared samples: (A) Ti–Ag, (B) PDA samples.

coating with rigid character and hierarchically micro/nano-textured surface topography was successfully developed.

Hydrophilicity analysis

In biological systems, the hydrophilicity of the implant surface plays a pivotal role in protein absorption and cell adhesion. The wettability of bare and modified Ti samples 24 h and 1 week subsequent to preparation were determined by CA measurements of sessile water drop, the result is presented in Table 1. As shown in the result, the dopamine polymerization had dramatically improved the hydrophilicity of TC4 according to the 24 h measurement, with the PDA30 samples showing the most wettable ability (almost completely spread water droplets). The result may prove that the reaction of dopamine polymerization was a litter easier on nano particles, showed better hydrophilicity with thicker Ag films, which is consistent with the SEM and XRD results. The hydrophilicity of modified surfaces tends to change with time and therefore their stability should also be studied. After one week's standing in air and immersed in DI water, the CA of TC4 changed slightly while that of the PDA samples altered differently. The PDA30 in DI water just increased by 5.0° compared with increased drastically by 31.5° in air. Nevertheless, the PDA samples just stand in air were still hydrophilic enough compared to TC4 (above 50°), especially PDA20 and PDA30. No to mention the PDA sample immersed in DI water, which can keep their excellent hydrophilicity property. The above weakening of CA in air might be a result of ubiquitous environmental contamination by adsorbing carbonaceous compounds at atmosphere conditions. Although, the polar groups (*e.g.* –OH, $-NH_2$) of the polydopamine layer could resist such pollution to some extent. It is still proposed to preserve the prepared PDA samples in DI water to keep its original hydrophilicity as prepared.

Ag^+ release in PBS

Fig. 6 displays the Ag^+ release time profiles from Ti–Ag and PDA samples in PBS. The total Ag content was 27.35 ± 1.13 μg, 54.65 ± 1.21 μg and 82.68 ± 1.46 μg for Ti–Ag10 (PDA10), Ti–Ag20 (PDA20) and Ti–Ag30 (PDA30). As shown in the figure, all the PDA samples had lower rate of Ag^+ release compared to Ti–Ag which had the same Ag layer thickness. These proved the main innovation of slow-released multilayer films that the top polydopamine layer reduced the release of Ag^+. After one month in PBS solution, the accumulative Ag^+ release of the PDA samples only took 25.5%, 16.7%, and 13.6% of the total Ag content for PDA10, PDA20, and PDA30 respectively. These demonstrated the prepared samples had excellent slow-release

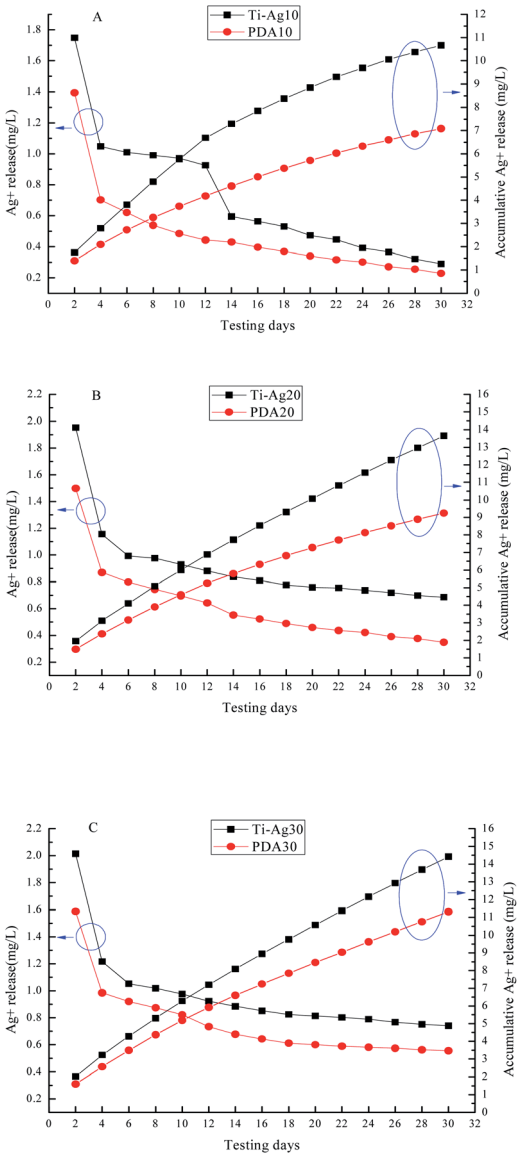

Fig. 6 The release behavior of silver in PBS: (A) Ti–Ag10 and PDA10, (B) Ti–Ag20 and PDA20, (C) Ti–Ag30 and PDA30.

effect. Compared to other samples, Ti–Ag-10's dissolution curve went a little different. It released more Ag^+ as expected in the first 12 days than PDA10, which could be caused by the discontinuous Ag layer would give out more Ag^+ at the beginning. In addition, excessive Ag^+ release may lead to some cytotoxicity, while the Ag^+ release concentrations of PDA samples in this study over 30 days were lower than both the

Table 1 The effects of surface modification on CA

	TC4	PDA10	PDA20	PDA30
Within 24 h (DI)	53.6 ± 1.53	16.6 ± 0.75	11.1 ± 0.51	10.0 ± 0.80
After one week (DI)	51.5 ± 1.65	24.3 ± 1.35	16.3 ± 0.79	15.0 ± 0.58
Within 24 h (air)	50.4 ± 2.55	20.3 ± 0.73	12.4 ± 0.50	11.6 ± 0.91
After one week (air)	51.1 ± 2.76	52.1 ± 2.01	45.6 ± 1.60	43.1 ± 1.88

biological safe concentration (1.6 mg L^{-1}) and toxic concentration (10 mg L^{-1}) of silver ions.

Antibacterial assessment

The silver nanoparticles loaded on the coating react with water to produce Ag^+, and due to diffusion, the Ag^+ will spread from the high concentration area to the low concentration area, thus killing bacteria or inhibiting bacterial proliferation, with a macroscopic expression of a translucent antibacterial ring. The antibacterial test result of the Ti–Ag and PDA samples is shown in Fig. 7. As proved by the ZOI results, the Ti–Ag samples presented good antibacterial activity both for *E. coli* and *S. aureus*. The tendency increased with the increasing of Ag thickness, which was caused more Ag^+ released from the prepared samples, correspond with the Ag^+ release results. It is obvious that *S. aureus* is more sensitive to the released Ag^+, the prepared samples can observe better antibacterial property for *S. aureus*. For the PDA samples, their antibacterial activity is not as good as the Ti–Ag samples, because of the covering of top dopamine layer. Such as PDA10, there is almost no antibacterial function for *E. coli*. But the other PDA samples still showed the acceptable antibacterial activity. The PDA samples' antibacterial results are also corresponding with Ag^+ release results, as higher Ag^+ released better antibacterial function would be observed. Considering the slow-release and satisfactory antibacterial functions, in the long run the PDA20 and PDA30 would be a good choice for antibacterial dental implant.

Cytocompatibility assessment

Evaluation of cytocompatibility is vital to evaluate whether a material is appropriate for biomedical applications.[37,38] As osteoblasts are existing at the root tip, a murine osteoblastic cell line (MC3T3-E1) was selected to co-culture with TC4 and PDA samples to demonstrate their biocompatibility by detecting the cell adhesion and viability. Cell adhesion has been a critical precondition for the subsequent interplay between coated materials and cells; such as cell morphology change, proliferation, recruitment, and differentiation.[39,40] MC3T3-E1 adhesion on all the samples for 24 h was examined by a double-label fluorescence staining of the actin cytoskeleton (red) and nucleus (blue). Fig. 8(A–D) presented that the seeded MC3T3-E1 cells in all the samples had a representative spindle-like morphology. Quantification in Fig. 8(E) proved that the cell density in PDA samples, was higher than that of the blank control. Especially the PDA20 and PDA30 samples, which may be caused by the excellent hydrophilicity property. The results also showed that the cell adhesion of PDA10 is not as high as another two PDA samples, even it has the similar hydrophilicity. In addition to the hydrophilic property, the cell adhesion might

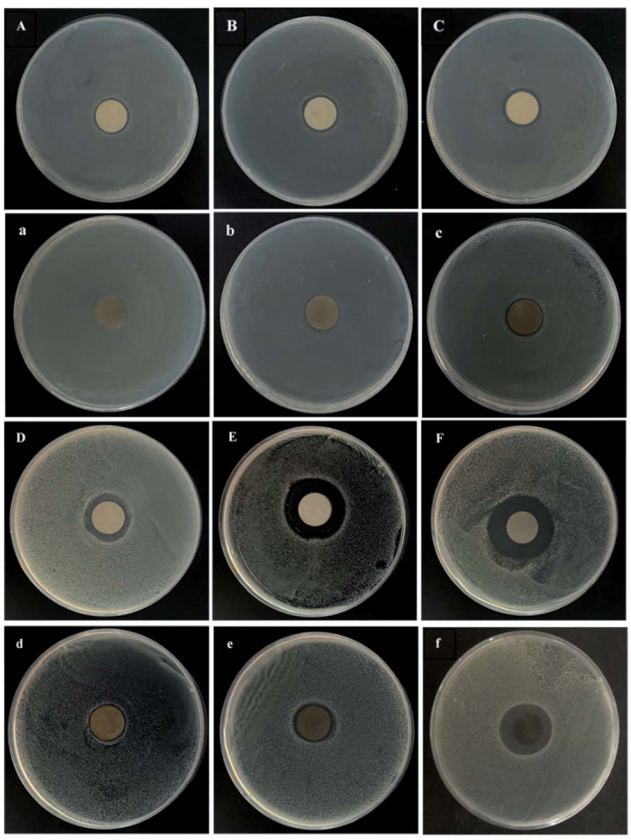

Fig. 7 Antibacterial properties of the prepared samples for *E. coli*. (A(a)–C(c)) and *S. aureus* (D(d)–F(f)): (A–C/D–F) Ti–Ag10–Ti–Ag30, (a–c/d–f) PDA10–PDA30.

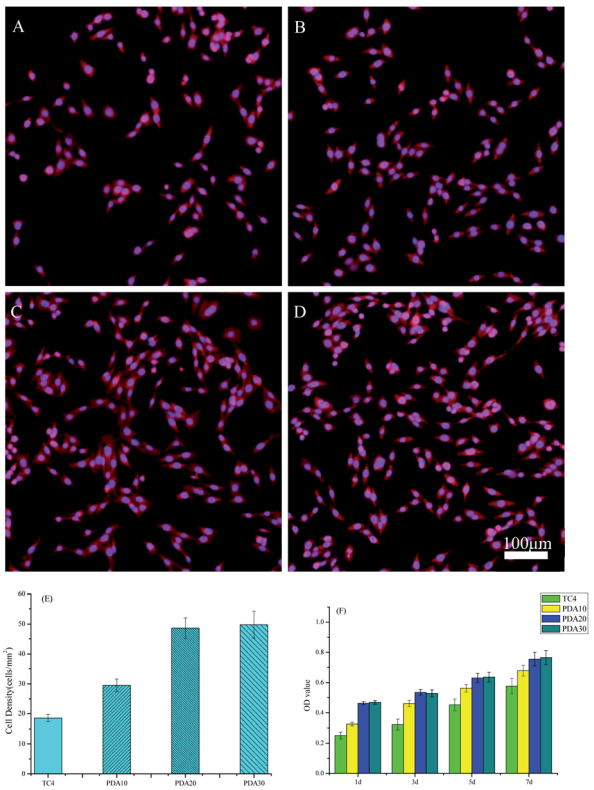

Fig. 8 Fluorescent images of MC3T3-E1 co-cultivation with TC4 (A), PDA10 (B), PDA20 (C), and PDA30 (D) for 24 h. Red is actin filaments visualized by TRITC-phalloidin staining, and blue is nuclei stained by DAPI; (E) density of cocultured MC3T3-E1for 24 h. (F) Cell viability of MC3T3-E1 after incubated with PDA samples.

be also affected by the surface structure. As shown in the SEM picture, the polydopamine deposited on PDA10 sample was small, not like the one on PDA20 and PDA30 samples, which were big and compacted.

As shown in Fig. 8(F), after 1 d, the cell viability on PDA samples was greatly higher than that of the TC4 sample, which is in line with the results of cell adhesion. As the incubation time increased from 1 to 7 d, the cell viability of all the samples significantly increased; taken all the results inconsideration, these results imply that the developed PDA samples possessed good cytocompatibility for great potential as implants.

Antibacterial biofilms for dental applications have attracted researchers' attentions, especially the slow-release antimicrobial implant coatings. For example, TiO_2–dopamine–Ag and TiO_2–Ag.[41–43] All the prepared samples have been proved to possess good antibacterial and cytocompatibility just as the samples we made in this research. But there is a big difference in Ag^+ release rate. With the similar testing method, after one month the Ag^+ release rate of our PDA samples is from 13%–25%, but the good TiO_2–dopamine–Ag is more than 90%. This result proved that our PDA samples will endure much more time, whose nano silver is protected by other film and will not release directly.

Conclusions

In this paper, we present a simple, controllable, and cost-effective method to produce biomimetic multilayer TC4–Ag–polydopamine coatings by combining magnetron sputtering techniques with mussel-inspired metallization. The resultant coatings exhibited slow-release of Ag^+, relevant antimicrobial potency, good MC3T3-E1 cells cytocompatibility. The coating processes are good in operability, repeatability, and workability regarding medical devices with complicated constructions and shapes, especially for the dental implant. Our preliminary findings would be helpful guidance to safe use of Ag coatings on dental implant.

Author contributions

The contributor roles are as follows: Hongmei Zhao-formal analysis and writing; Na Bai-data curation; Qian Zhang-investigation; Ying Wang-methodology; Wenjing Jiang-methodology; Jianjun Yang-funding acquisition and supervision.

Conflicts of interest

There are no conflicts to declare.

Acknowledgements

We gratefully acknowledge the project: 21-1-4-rkjk-20-nsh.

References

1 L. Tan, X. Yu, W. Peng and Y. Ke, *J. Mater. Sci. Technol.*, 2013, **29**, 503.
2 C. Hu, D. Ashok, D. R. Nisbet and V. Gautam, *Biomaterials*, 2019, **219**, 119366.
3 D. A. Florea, D. Albulet, A. M. Grumezescu and E. Andronescu, *Mater. Chem. Phys.*, 2020, **243**, 11.
4 B. Mcentire, B. Bal, M. Rahaman, J. Chevalier and G. Pezzotti, *J. Eur. Ceram. Soc.*, 2015, **35**, 4327.
5 H. Dreyer, J. Grischke, C. Tiede, J. Eberhard, A. Schweitzer, S. E. Toikkanen, S. Glockner, G. Krause and M. Stiesch, *J. Periodontal Res.*, 2018, **53**, 657.
6 M. Hultin, A. Gustafsson, H. Hallström, L. A. Johansson, A. Ekfeldt and B. Klinge, *Clin. Oral Implants Res.*, 2010, **13**, 349.
7 N. P. Lang and T. Berglundh, *J. Clin. Periodontol.*, 2011, **38**, 178.
8 L. W. Lindquist, G. E. Carlsson and T. A. Jemt, Clinical results and marginal bone loss, *Clin. Oral Implants Res.*, 1997, **7**, 329.
9 B. E. Pjetursson, K. Tan, N. P. Lang, U. Bragger, M. Egger and M. Zwahlen, *Clin. Oral Implants Res.*, 2004, **15**, 625.
10 R. N. Salaie, A. Besinis, H. Le, C. Tredwin and R. Handy, *Mater. Sci. Eng., C*, 2020, **107**, 110210.
11 C. Dini, B. E. Nagay, J. M. Cordeiro, N. Cruz and V. Baro, *Mater. Sci. Eng., C*, 2020, **110**, 110657.
12 Z. Xu, S. Krajewski, T. Weindl, R. Loeffler, P. Li, X. Han, J. Geis-Gerstorfer, H. P. Wendel, L. Scheideler and F. Rupp, *Mater. Sci. Eng., C*, 2020, **110**, 110701.
13 L. García-Fernández, J. Cui, C. Serrano, Z. Shafiq, R. Gropeanu, V. San Miguel, J. Iturri, M. Wang, G. Auernhammer, S. Ritz, A. Golriz, R. Berger, M. Wagner and A. Campo, *Adv. Mater.*, 2013, **25**, 529.
14 F. Cao, E. Ju, Z. Yan, Z. Wang and X. Qu, *ACS Nano*, 2017, **11**, 4651.
15 P. Anjana, M. Bindhu, M. Umadevi and R. Rakhi, *Appl. Surf. Sci.*, 2019, **479**, 96.
16 D. Qin, G. Yang, Y. Wang, Y. Zhou and L. Zhang, *Appl. Surf. Sci.*, 2019, **469**, 528.
17 Q. L. Feng, J. Wu, G. Q. Chen, F. Z. Cui and J. O. Kim, *J. Biomed. Mater. Res.*, 2000, **52**, 662.
18 L. Bonilla-Gameros, P. Chevallier, A. Sarkissian and D. Mantovani, *Nanomedicine*, 2019, **24**, 102142.
19 B. Reidy, A. Haase, A. Luch, K. A. Dawson and I. Lynch, *Materials*, 2013, **6**, 2295.
20 Z. Meran, A. Besinis, T. De Peralta and R. D. Handy, *J. Biomed. Mater. Res., Part B*, 2018, **106**, 1038.
21 L. Li and H. Zeng, *Biotribology*, 2016, **5**, 44.
22 A. Jin, Y. Wang, K. Lin and L. Jiang, *Bioact. Mater.*, 2020, **5**, 522.
23 A. Cholewinski, F. Yang and B. Zhao, *Mater. Horiz.*, 2019, **6**, 285.
24 C. Liu, J. Liu, X. Ning, S. Chen and D. Miao, *Polymers*, 2019, **11**, 627.
25 G. Mondin, F. M. Wisser, A. Leifert, N. Mohamed-Noriega, J. Grothe, S. Dörfler and S. Kaskel, *J. Colloid Interface Sci.*, 2013, **411**, 187.
26 J. Tian, G. Yang, H. Huang, M. Liu and Y. Wei, *J. Environ. Chem. Eng.*, 2020, **8**, 104383.
27 Z. Zhe, Z. Jing, B. Zhang and J. Tang, *Nanoscale*, 2015, **5**, 118.

28 Y. Cong, T. Xia, M. Zou, Z. Li, B. Peng, D. Guo and Z. Deng, *J. Mater. Chem. B*, 2014, **2**, 3450.
29 Y. Liao, B. Cao, W. C. Wang, L. Zhang, D. Wu and R. Jin, *Appl. Surf. Sci.*, 2009, **255**, 8207.
30 V. Ball, I. Nguyen, M. Haupt, C. Oehr and D. Ruch, *J. Colloid Interface Sci.*, 2011, **364**, 359.
31 D. Fu, Y. Lu, S. Gao, Y. Peng and H. Duan, *J. Wuhan Univ. Technol., Mater. Sci. Ed.*, 2019, **34**, 968.
32 Z. Jia, P. Xiu, M. Li, X. Xu, Y. Shi, Y. Cheng, S. Wei, Y. Zheng, T. Xi, H. Cai and Z. Liu, *Biomaterials*, 2016, **75**, 203.
33 X. Zhang, S. Jiang, M. Cai, H. Zhao, F. Pan, D. Miao and X. Ning, *Ceram. Int.*, 2020, **46**, 13342.
34 Y. Peng, J. Li, Y. Du, J. Xiong and J. Shi, *Vacuum*, 2021, **187**, 110134.
35 X. Liu, J. Cao, H. Li, J. Li, Q. Jin, K. Ren and J. Ji, *ACS Nano*, 2013, **7**, 9384.
36 K. Black, J. Yi, J. Rivera, D. Zelasko-Leon and P. Messersmith, *Nanomedicine*, 2013, **8**, 17.
37 Y. Hao, W. Zhao, L. Zhang, X. Zeng, Z. Sun, D. Zhang, P. Shen, Z. Li, Y. Han and P. Li, *Mater. Des.*, 2020, **193**, 108863.
38 Y. He, W. Zhao, Z. Dong, Y. Ji, M. Li, Y. Hao, D. Zhang, C. Yuan, J. Deng and P. Zhao, *Int. J. Biol. Macromol.*, 2021, **167**, 182.
39 Q. Zhou, L. Ge, C. Guimarães, P. Kühn, L. Yang and P. Rijn, *Adv. Mater. Interfaces*, 2018, **5**, 1800504.
40 Q. Zhou, Z. Zhao, Z. Zhou, G. Zhang, R. Chiechi and P. Rijn, *Adv. Mater. Interfaces*, 2018, **5**, 1800334.
41 J. Li, X. Liu, Y. Qiao, H. Zhu and C. X. Ding, *Colloids Surf., B*, 2014, **113**, 134.
42 S. Mei, H. Wang, W. Wang, L. Tong, H. Pan and C. Ruan, *Biomaterials*, 2014, **35**, 4255.
43 A. Gao, R. Hang, X. Huang, L. Zhao, X. Zhang and L. Wang, *Biomaterials*, 2014, **35**, 4223.